

SANDIA REPORT

SAND2012-2938

Unlimited Release

Printed April 2012

First principles predictions of intrinsic defects in aluminum arsenide, AlAs: Numerical Supplement

Peter A. Schultz

Prepared by
Sandia National Laboratories
Albuquerque, New Mexico 87185 and Livermore, California 94550

Sandia National Laboratories is a multi-program laboratory managed and operated by Sandia Corporation, a wholly owned subsidiary of Lockheed Martin Corporation, for the U.S. Department of Energy's National Nuclear Security Administration under contract DE-AC04-94AL85000.

Approved for public release; further dissemination unlimited.



Sandia National Laboratories

Issued by Sandia National Laboratories, operated for the United States Department of Energy by Sandia Corporation.

NOTICE: This report was prepared as an account of work sponsored by an agency of the United States Government. Neither the United States Government, nor any agency thereof, nor any of their employees, nor any of their contractors, subcontractors, or their employees, make any warranty, express or implied, or assume any legal liability or responsibility for the accuracy, completeness, or usefulness of any information, apparatus, product, or process disclosed, or represent that its use would not infringe privately owned rights. Reference herein to any specific commercial product, process, or service by trade name, trademark, manufacturer, or otherwise, does not necessarily constitute or imply its endorsement, recommendation, or favoring by the United States Government, any agency thereof, or any of their contractors or subcontractors. The views and opinions expressed herein do not necessarily state or reflect those of the United States Government, any agency thereof, or any of their contractors.

Printed in the United States of America. This report has been reproduced directly from the best available copy.

Available to DOE and DOE contractors from
U.S. Department of Energy
Office of Scientific and Technical Information
P.O. Box 62
Oak Ridge, TN 37831

Telephone: (865) 576-8401
Facsimile: (865) 576-5728
E-Mail: reports@adonis.osti.gov
Online ordering: <http://www.osti.gov/bridge>

Available to the public from
U.S. Department of Commerce
National Technical Information Service
5285 Port Royal Rd.
Springfield, VA 22161

Telephone: (800) 553-6847
Facsimile: (703) 605-6900
E-Mail: orders@ntis.fedworld.gov
Online order: <http://www.ntis.gov/help/ordermethods.asp?loc=7-4-0#online>



SAND2012-2938
Unlimited Release
Printed April 2012

First principles predictions of intrinsic defects in aluminum arsenide, AlAs: Numerical Supplement

Peter A. Schultz
Advanced Device Technologies, Dept. 1425
Sandia National Laboratories
P.O. Box 5800
Albuquerque, New Mexico 87185-MS1322

Abstract

This Report presents numerical tables summarizing properties of intrinsic defects in aluminum arsenide, AlAs, as computed by density functional theory. This Report serves as a numerical supplement to the results published in: P.A. Schultz, "First principles predictions of intrinsic defects in Aluminum Arsenide, AlAs", Materials Research Society Symposia Proceedings **1370** (2011; SAND2011-2436C), and intended for use as reference tables for a defect physics package in device models.

This page intentionally left blank

CONTENTS

First principles predictions of intrinsic defects in aluminum arsenide, AlAs: Numerical Supplement	3
1. Introduction.....	7
1.1. Computational methods	7
1.2. Verification and validation	7
1.2.1. Extrapolation model	8
1.2.2. Validation of AlAs defect results	9
2. Results.....	11
2.1. Defect atomic structures	11
2.2. Defect charge transition energy levels.....	12
2.3. Defect formation energies.....	15
2.4. Defect migration energies	16
2.4.1. Aluminum interstitial – thermal	16
2.4.2. Arsenic interstitial – thermal	16
2.4.3. Athermal and recombination enhanced diffusion: arsenic interstitial	17
3. Conclusions.....	19
4. References.....	19

TABLES

Table 1. Computed bulk AlAs properties	8
Table 2. Supercell extrapolation energies, $\epsilon_0=10.1$, $R_{\text{skin}}=1.4$ bohr.....	9
Table 3. Ground state structure designations for vacancy and antisite defects.	11
Table 4. Ground state structure designations for the interstitials and di-antisite.....	11
Table 5. Defect levels for the aluminum vacancy, in eV, referenced to the VBE: $v_{\text{Al}}(v') \leftrightarrow v_{\text{As}}-a_{\text{Al}}(v^*)$	12
Table 6. Defect levels for the arsenic vacancy, in eV, referenced to the VBE: $v_{\text{As}}(v') \leftrightarrow v_{\text{Al}}-a_{\text{As}}(v^*)$	12
Table 7. Defect levels for the divacancy, in eV, referenced to the VBE: $vv = v_{\text{As}}-v_{\text{Al}}$	12
Table 8. Defect levels for the arsenic antisite, in eV, referenced to the VBE: $a_{\text{As}} = a_{\text{Al}}$	13
Table 9. Defect levels for the aluminum antisite, in eV, referenced to the VBE: $a_{\text{Al}} = a_{\text{As}}$	13
Table 10. Defect levels for the di-antisite, in eV, referenced to the VBE: $aa = a_{\text{Al}}-a_{\text{As}}$	13
Table 11. Defect levels for the aluminum interstitial, in eV, referenced to the VBE: $i_{\text{Al}} = i_{\text{As}}$	14
Table 12. Defect levels for the arsenic interstitial, in eV, referenced to the VBE: $i_{\text{As}} = i_{\text{Al}}$	14
Table 13. Formation energies of AlAs defects at VBE, in eV, context = LDA.	15
Table 14. Formation energies of AlAs defects at VBE, in eV, context = PBE.	15
Table 15. Diffusion barriers (thermal) for the aluminum interstitial, in eV.	16
Table 16. Diffusion barriers (thermal) for the arsenic interstitial, in eV.	17

NOMENCLATURE

CBE	conduction band edge
DFT	density functional theory
eV	electron Volt
FDSM	finite defect supercell model
GGA	generalized gradient approximation
IP	ionization potential
LDA	local density approximation
LMCC	local moment countercharge
MRS	Materials Research Society
MSMSE	Modelling and Simulation in Materials Science and Engineering
n/c	not computed
n/x	not exist
PAS11	Article: P.A. Schultz, MRS Symp. Proc 1370 (in press), SAND2011-2436C.
PBE	Perdew/Burke/Ernzerhof, a “flavor” of GGA
PP	pseudopotential
SNL	Sandia National Laboratories
VBE	valence band edge

1. INTRODUCTION

The numerical results for density functional theory (DFT) calculations of properties of simple intrinsic defects aluminum arsenide are presented. This condenses the results published in the Proceedings of the Materials Research Society (MRS) 2011 Spring Meeting: “First principles predictions of intrinsic defects in aluminum arsenide, AlAs”, P.A. Schultz. MRS Symposia Proceedings, Vol. 1370 (2011), SAND2011-2436C (henceforth “PAS11”). [1] The results of the defect calculations are summarized into a series of numerical Tables containing the parameters needed to populate defect physics packages needed for device simulations. In addition, a summary of the AlAs-specific verification and validation evidence is presented that provides a basis for estimating an overall uncertainty in predicted defect energy levels of the same size as for earlier simulations of silicon defects [2] and GaAs defects [3] (henceforth “PAS09”), namely, 0.1-0.2 eV accuracy/uncertainty.

1.1. Computational methods

Details of the computational methods are described in PAS11 and also in the description of GaAs defect calculations [3], and will only be briefly summarized here. The DFT calculations were performed with the SEQQUEST DFT code. [4]. The defect calculations were performed using both the local density approximation (LDA) [5] and the Perdew-Burke-Ernzerhof (PBE) flavor of the generalized gradient approximation [6], this comparison being a partial assessment of the physical uncertainties within DFT functionals [7]. The calculations used $Z=3$ valence pseudopotentials (PP) for the Al atom (without a partial core correction), and $Z=5$ valence PP for the As atom, the latter being the same used for GaAs defects, [3], i.e. an extended PP with the f -potential used as the local potential and also including a partial core correction.

The calculations of charged defects used the Finite Defect Supercell Model [2] to incorporate rigorous boundary conditions for the solution of the electrostatic potential in a charged supercell [8] and extrapolate the computed defect energies to the infinitely dilute limit. Defect calculations were performed using 64-atom, 216-atom, and 512-atom cubic supercells. The 216-site supercell calculations proved to be sufficiently converged to achieve the required accuracy and are the default production calculations listed in this Report.

These simulation contexts are labeled in the following as: LDA64, LDA, and LDA512, for 64-site, 216-site, and 512-site, respectively, supercell calculations using LDA; and PBE for the 216-site supercells using PBE.

1.2. Verification and validation

The defect level calculations all used the same methods, SEQQUEST invoking FDSM, used in DFT calculations of defects in silicon and GaAs, which yielded mean absolute errors of 0.1 eV and maximum absolute error of 0.2 eV for defect levels (and other properties) over a wide sampling of different defects. This is the expected accuracy (uncertainties) of the methods for the AlAs defect level calculations, and certainly are the limit of the physical accuracy of the DFT approximations used in this analysis.

The pseudopotentials used in the AlAs calculations were extensively verified in previous studies, the As in the GaAs calculations [9,3], and the Al in calculations of bulk Al defects [10], and

validated for the bulk crystalline calculations. The properties of bulk (zinc-blende structure) AlAs obtained with these simulation contexts are summarized in the following Table.

Table 1. Computed bulk AlAs properties

Simulation context	Lattice parameter (Å)	Bulk Modulus (GPa)	Kohn-Sham Band gap (eV)	Formation energy (eV)
Experiment	5.66 (a)	74(4) (b)	2.2 (c)	1.21 (d)
LDA	5.622	75	1.37	0.930
PBE	5.843	66	1.53	0.951

(a) Ref. [11].

(b) Ref. [12].

(c) Ref. [13].

(d) Ref. [14].

Comparison of AlAs defect level results with different functionals, LDA vs. PBE, indicates a modest uncertainty due to the physical approximation of DFT. The largest differences in a defect level are 0.28 eV in the $\nu\nu(1-/0)$ transition and 0.18 eV for the $\nu_{As}(2+/1+)$ transition, but the rest are typically (much) less than 0.1 eV, sufficiently similar to plot usefully on the same level diagram, see Fig. 1 in PAS11. The AlAs defects, like the GaAs defects are predicted to have multiple $-U$ transitions and structural rearrangements with change in charge state, suggesting that PBE might be necessary to achieve the 0.1-0.2 eV target accuracy seen in computations of defect levels in silicon (and in GaAs).

1.2.1. Extrapolation model

The total energy calculations for the charged defects used a modified-Jost model [15, 2] to evaluate the missing charge polarization (screening) energy outside the finite volume of the supercell:

$$E_{pol} = (1 - 1/\epsilon_0) q^2/R_{Jost} \quad (1)$$

where ϵ_0 is the static dielectric constant, and $R_{Jost} = (R_{sphere} - R_{skin})$ is the radius of a sphere with a volume equal to the volume of the supercell, R_{sphere} , less the skin depth, R_{skin} , of an unscreened surface region within the sphere. R_{skin} must be calibrated (fit) once for each material system.

The *extrapolation model* was *calibrated* via calculations of negative charge states of the aluminum vacancy, in unrelaxed tetrahedral structures for the (1-), (2-), and (3-) charge states.

The *extrapolation model* was then *verified* using fully relaxed arsenic antisite (0/1+) and (1+/2+) charge transitions, comparing defect calculations extrapolated to infinitely dilute defects from 64-site, from 216-site, and from 512-site supercell calculations. 216-site cells were assessed to be necessary to meet required level of quantitative confidence. The $\nu\nu$ divacancy (as an example of a low-symmetry defect expected to have large spatial extent) with 216-site supercells was repeated using 512-site supercells as a further verification test. The differences in any defect level was typically smaller than 0.05 eV, indicating uncertainty with respect to cell size (and k-point sampling) is less than 0.05 eV, except for large ~ 0.1 uncertainties in the extreme charge states (of the $\nu\nu$).

The *extrapolation model* was *validated*. The experimental AlAs static dielectric constant, [16] 10.1, for ϵ_0 and a physically reasonable unpolarized “skin depth” (R_{skin}), 1.4 bohr, led to a converged extrapolation, and these parameters are also consistent with extrapolation models in multiple other III-V defect calculations such as GaAs, InP, and GaP (experimental ϵ_0 and $R_{\text{skin}}=1.5(2)$)

The quantities defining the extrapolation model are summarized in the next Table.

Table 2. Supercell extrapolation energies, $\epsilon_0=10.1$, $R_{\text{skin}}=1.4$ bohr.

Context:	LDA64	LDA512	LDA	PBE
$a_0(\text{\AA})$	5.622	5.622	5.622	5.738
IP(VBE) (eV)	7.05	7.15	7.27	6.60
Charge	External polarization energy (eV), Eq. 1			
$ q = 1$	1.0404	0.4910	0.6672	0.6528
$ q = 2$	4.1617	1.9641	2.6687	2.6111
$ q = 3$	9.3638	4.4193	6.0047	5.8750
$ q = 4$	16.6468	7.8566	10.6750	10.4444

1.2.2. Validation of AlAs defect results

The amount of data available to quantitatively validate AlAs defect results is miniscule in comparison to GaAs, already small in comparison to Si. To date, there are no measured defect levels firmly identified with any point defect charge transition. The range of computed defect levels, ~ 2.7 eV, is significantly larger than the experimental band gap, suggesting either (1) that the defect level calculations in AlAs have larger uncertainties (relative to one another) than in the other III-V binaries, or (2) the valence band edge and conduction band edge cut through the top and/or bottom of the range of defect levels (either the levels are resonances in the CB or VB, or the computed levels are not cleanly associated with localized states). The current state of experimental knowledge is insufficient to calibrate the position of the band edges. This assessment of the quality of the validation of these computed results requires that additional data for AlAs defects be acquired. The calculation of defect formation energies, being dependent upon the position of the VBE with respect to the defect levels, would need to be revisited once the band edges are properly calibrated to experimental data.

This page intentionally left blank

2. RESULTS

The section contains the Tables that summarize the numerical results for DFT simulations of defects in AlAs.

2.1. Defect atomic structures

The following Tables list the ground state structures for the simple intrinsic defects in AlAs as a function of charge state. The bonding structures are all illustrated in PAS09. In the vacancies, note the distinction that v' refers to the simple vacancy, and v^* refers to the site-shifted form of the vacancy (where a nearest-atom to the vacancy hops into the vacant site, thus creating a vacancy-antisite pair).

Table 3. Ground state structure designations for vacancy and antisite defects.

Charge state	$v' = v_{Al} \leftrightarrow v^* = v_{As}As_{Al}$	$v' = v_{As} \leftrightarrow v^* = v_{Al}Al_{As}$	vv	aAs	aAl
(4-)	-	-	$C_{1h}\text{-pair}(Al)$	-	-
(3-)	v'/T_d	v^*/C_{3v}	$C_{1h}\text{-pair}(Al)$	-	-
(2-)	$v'/\sim T_d$	$v'/\text{pair-}D_{2d}$ $v^*/\text{pair-}C_{1h} \{pbe\}$	$C_{3v}\text{-in}(Al)$ $C_{1h}\text{-pair}(Al) \{lda512\}$	$*C_{3v}$	T_d
(1-)	$v'/\sim T_d$	$v'/\text{pair-}D_{2d}$	$C_{3v}\text{-in}(Al)$	$*C_{3v}$	$res\text{-}D_{2d}$
(0)	$v'/\sim T_d$	$v'/\text{pair-}D_{2d}$	$C_{3v}\text{-out}(Al)$	T_d	$res\text{-}D_{2d}$
(1+)	$v^*/C_{3v}\text{-in}(Al)$	$v'/T_d\text{-in}(Al)$	$\sim C_{3v}\text{-out}(Al)$	T_d	$pair\text{-}D_{2d}$
(2+)	$v^*/C_{3v}\text{-out}(Al)$	$v'/T_d\text{-out}(Al)$	$\sim C_{3v}\text{-out}(Al)$	T_d	$pair\text{-}D_{2d}$
(3+)	$v^*/C_{3v}\text{-out}(Al)$	$v'/T_d\text{-out}(Al)$	$\sim C_{3v}\text{-out}(Al)$	-	T_d
(4+)	-	-	$\sim C_{3v}\text{-out}(Al)$	-	T_d

Table 4. Ground state structure designations for the interstitials and di-antisite.

Charge state	Al_i	As_i	aa
(2-)	-	-	C_{3v}
(1-)	$C_{2v} \text{ split-}(110)_{Al}$	$C_{2v} \text{ split-}110_{As}$	C_{3v}
(0)	$C_{2v} \text{ split-}(110)_{Al}$	$C_{2v} \text{ split-}110_{As}$	C_{3v}
(1+)	$T_{i,Al}$	$C_{1h} \text{ p-}(001)_{Al}$	$pair\text{-}C_{1h}$
(2+)	$T_{i,As}$	$C_{1h} B_{Al}$	$pair\text{-}C_{1h}$
(3+)	$T_{i,As}$	$T_{i,Al}$	$pair\text{-}C_{1h}$
(4+)	-	-	C_{3v}

2.2. Defect charge transition energy levels

This section presents the defect charge transition levels of the simple intrinsic defects in AlAs, in eV, along with the neutral formation energies. The defect level calculations are the primary result of the Report, the later formation energies are all derived from these results.

Table 5. Defect levels for the aluminum vacancy, in eV, referenced to the VBE:

$$v_{Al} (v') \leftrightarrow v_{As}-As_{Al} (v^*)$$

V_{Al} Context	Neutral formation energy	Defect levels (eV), cf. VBE						
		(3+/2+)	(2+/1+)	(1+/0)	(0/1-)	(1-/2-)	(2-/3-)	(3-/4-)
Unrelaxed T_d - v' (for polarization calibration)								
LDA64	3.604	n/c	n/c	n/c	1.081	1.543	2.028	n/x
LDA	3.746	n/c	n/c	n/c	1.105	1.548	2.039	n/x
LDA512	3.812	n/c	n/c	n/c	1.095	1.545	2.040	n/x
Relaxed thermodynamic levels								
LDA	3.48	0.83	0.41	1.32	0.95	1.22	1.52	n/x
PBE	3.30	0.99	0.56	1.27	0.97	1.24	1.53	n/x

Table 6. Defect levels for the arsenic vacancy, in eV, referenced to the VBE:

$$v_{As} (v') \leftrightarrow v_{Al}-Al_{As} (v^*)$$

V_{As} Context	Neutral formation energy	Defect levels (eV), cf. VBE						
		(3+/2+)	(2+/1+)	(1+/0)	(0/1-)	(1-/2-)	(2-/3-)	(3-/4-)
LDA	4.08	0.71	0.22	1.62	1.32	2.44	2.17	n/x
PBE	4.10	0.90	0.40	1.68	1.33	2.46	2.08	n/x

Table 7. Defect levels for the divacancy, in eV, referenced to the VBE:

$$vv = v_{As}-v_{Al}$$

vv Context	Neutral formation energy	Defect levels (eV), cf. VBE							
		(4+/3+)	(3+/2+)	(2+/1+)	(1+/0)	(0/1-)	(1-/2-)	(2-/3-)	(3-/4-)
LDA512	4.86	n/c	0.30	0.53	0.78	1.34	1.22	2.47	2.57
LDA	4.83	0.02	0.19	0.50	0.78	1.37	1.24	2.50	2.65
PBE	4.42	0.06	0.23	0.54	0.81	1.65	1.25	2.49	2.63

Table 8. Defect levels for the arsenic antisite, in eV, referenced to the VBE:
 $aAs = As_{Al}$

As_{Al} Context	Neutral formation energy	Defect level (eV), cf. VBE						
		(3+/2+)	(2+/1+)	(1+/0)	(0/1-)	(1-/2-)	(2-/3-)	(3-/4-)
LDA64	1.414	n/x	0.933	1.239	n/c			
LDA512	1.403	n/x	0.928	1.243	n/c			
LDA	1.402	n/x	0.927	1.240	2.51	2.19	n/x	
PBE	1.23	n/x	0.92	1.23	2.60	2.24	n/x	

Table 9. Defect levels for the aluminum antisite, in eV, referenced to the VBE:
 $aAl = Al_{As}$

Al_{As} Context	Neutral formation energy	Defect level (eV), cf. VBE						
		(4+/3+)	(3+/2+)	(2+/1+)	(1+/0)	(0/1-)	(1-/2-)	(2-/3-)
LDA	4.95	0.05	0.23	0.65	0.96	1.98	2.07	n/x
PBE	4.80	0.09	0.28	0.68	0.87	1.41	1.72	n/x

Table 10. Defect levels for the di-antisite, in eV, referenced to the VBE:
 $aa = Al_{As}-As_{Al}$

aa Context	Neutral formation energy	Defect levels (eV), cf. VBE						
		(4+/3+)	(3+/2+)	(2+/1+)	(1+/0)	(0/1-)	(1-/2-)	(2-/3-)
LDA	4.11	0.08	0.30	0.65	0.96	1.98	2.07	n/x
PBE	3.91	0.12	0.34	0.67	0.98	1.97	2.08	n/x

Table 11. Defect levels for the aluminum interstitial, in eV, referenced to the VBE:
 $iAl = Al_i$

Al_i Context	Neutral formation energy	Defect levels (eV), cf. VBE						
		(3+/2+)	(2+/1+)^(a) ($T_{i,Al}[+]$)	(1+/0)^(a) ($T_{i,Al}[+]$)	(0/1-)	(3+/2+)	(2+/1+)^(b) ($T_{i,As}[+]$)	(1+/0)^(b) ($T_{i,As}[+]$)
LDA	4.37	1.14	0.84	2.37	1.71	1.14	1.40	1.81
PBE	4.45	1.13	0.91	2.43	1.74	1.13	1.38	1.96

(a) Thermodynamic levels traversing charge state ground states: $T_{i,Al}(1+)-T_{i,As}(2+)-T_{i,As}(3+)$.

(b) Levels of the Al_i trapped in the $T_{i,As}$ site (i.e., excluded from the $T_{i,Al}(+)$ ground state).

Table 12. Defect levels for the arsenic interstitial, in eV, referenced to the VBE: $iAs = As_i$

As_i Context	Neutral formation energy	Defect levels (eV), cf. VBE						
		(3+/2+)	(2+/1+)	(1+/0)	(0/1-)	(1-/2-)	(2-/3-)	(3-/4-)
LDA	3.40	0.80	0.35	1.47	1.21	n/x		
PBE	3.36	0.76	0.36	1.51	1.29	n/x		

2.3. Defect formation energies

The ground state defect formation energies, as a function of charge state are trivially obtained by simple arithmetic from the neutral formation energies and the computed defect charge transition energy levels in the previous section. As all the results in this Report, the defect formation energies in these Tables are presented in the arsenic-rich limit. The formation energies of the charged defects are presented with the Fermi level at the VBE. The Tables present the formation energies of all the simple intrinsic defects, segregated by simulation context.

The aluminum interstitial quotes two formation energies for the (1+) charge, the first is the ground state of the (1+) state in the non-bond tetrahedral interstitial site with Al nearest neighbors: $T_{i,Al}$. The $T_{i,As}$ has charge states from (1+) through (3+), and is the ground state for the (2+) and (3+), and therefore its formation energy is also quoted.

Table 13. Formation energies of AIAs defects at VBE, in eV, context = LDA.

Charge state	vAl	vAs	vv	aAs	aAl	aa	iAl $T_{i,Al}; T_{i,As}$	iAs
(4-)	-	-	12.59	-	-	-	-	-
(3-)	7.17	10.01	9.94	-	-	-	-	-
(2-)	5.65	7.84	7.44	6.10	9.00	8.16	-	-
(1-)	4.43	5.40	6.20	3.91	6.93	6.09	6.08	4.61
(0)	3.48	4.08	4.83	1.40	4.95	4.11	4.37	3.40
(1+)	2.16	2.46	4.05	0.16	3.99	3.15	2.00;2.56	1.93
(2+)	1.75	2.24	3.55	-0.77	3.34	2.50	1.16	1.58
(3+)	0.92	1.53	3.36	-	3.11	2.20	0.02	0.78
(4+)	-	-	3.34	-	3.06	2.12	-	-

Table 14. Formation energies of AIAs defects at VBE, in eV, context = PBE.

Charge state	vAl	vAs	vv	aAs	aAl	aa	iAl $T_{i,Al}; T_{i,As}$	iAs
(4-)	-	-	12.44	-	-	-	-	-
(3-)	7.04	9.97	9.81	-	-	-	-	-
(2-)	5.51	7.89	7.32	6.07	4.58	7.96	-	-
(1-)	4.27	5.43	6.07	3.83	3.80	5.88	6.19	4.65
(0)	3.30	4.10	4.42	1.23	4.80	3.91	4.45	3.36
(1+)	2.03	2.42	3.61	0.00	3.93	2.93	2.02;2.49	1.85
(2+)	1.47	2.02	3.07	-0.92	3.25	2.26	1.11	1.49
(3+)	0.48	1.12	2.84	-	2.97	1.92	-0.02	0.73
(4+)	-	-	2.78	-	2.88	1.80	-	-

2.4. Defect migration energies

Only two intrinsic defects are potentially mobile: the Al_i and As_i . All other defects will be immobile at room or operating temperature (certainly for the time scales of interest for radiation damage). In addition to potential thermal diffusion, the As_i might exhibit athermal diffusion [17] (via carrier-driven Bourgoin-Corbett diffusion [18]) in p -type AlAs, and potentially recombination-enhanced diffusion in n -type AlAs, just as in GaAs.

2.4.1. Aluminum interstitial – thermal

For the Al interstitial, the DFT calculations finding thermodynamically stable states for the same (1+), (2+), and (3+) charge states seen for the Ga interstitial in GaAs, and also (0) and (1-) charges states in the split-(110)_{Al} interstitial now are stable defects in the gap. The positive interstitials strongly favor non-bonded tetrahedral interstitial positions over all other structures, and both $T(0)$ defects are deeply embedded in the conduction band.

The aluminum interstitial could potentially migrate thermally in p -type AlAs, through either the hexagonal site (via a $T_{i,\text{As}}-H-T_{i,\text{Al}}-H-T_{i,\text{As}}$ path) or through a split-(110)_{Al} site kick-through mechanism. The hexagonal path remains a clean defect state in the DFT calculations, allowing the full cannot be fully characterized for the (2+) and (3+) charge states, as the defect Kohn-Sham eigenstate dips below the VBE for the $T_{i,\text{Al}}(2+;3+)$ and a rigorous defect energy cannot be computed with current methods, but it can be unambiguously identified as a local minimum basin through which the interstitial could traverse.

Table 15. Diffusion barriers (thermal) for the aluminum interstitial, in eV.

Pathway:	Hexagonal site (H)			Split-(110) _{Al} site		
Context	$\text{Al}_i(1+)$	$\text{Al}_i(2+)$	$\text{Al}_i(3+)$	$\text{Al}_i(1+)$	$\text{Al}_i(2+)$	$\text{Al}_i(3+)$
LDA	1.26	0.80	1.04	0.87	0.81	1.35
PBE	1.21	0.81	0.99	0.89	0.86	1.36

2.4.2. Arsenic interstitial – thermal

Migration paths and barriers for the As interstitial were only obtained for p -type AlAs, an incidental byproduct of a comprehensive search for ground state structures. The thermal barrier for migration for the $\text{As}_i(3+)$ migration is 0.7-1.0 eV via a non-bonded $T_{i,\text{As}}-H-T_{i,\text{Al}}$ pathway, the hexagonal (H) site being the saddle point between the lower-energy T sites. Unlike GaAs, the defect states stay cleanly above the VBE throughout this path. This is a notably higher barrier for the $\text{As}_i(3+)$ than in GaAs, but still potentially accessible via thermal processes.

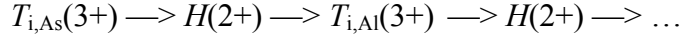
The thermal barrier for $\text{As}_i(2+)$ is estimated to be smaller, 0.6 eV, assuming net migration along the same pathway, except that the B_g -site is the ground state for the $\text{As}_i(2+)$, not the H -site. This estimate assumes the barrier to move from the B_g -site into the non-bonded $T-H-T$ pathway does not exceed 0.6 eV. This was not verified in these calculations, and would need to be investigated via NEB calculations. There is no information from experiment concerning interstitial mobility.

Table 16. Diffusion barriers (thermal) for the arsenic interstitial, in eV.

	As_i(2+) 0.6 eV				As_i(3+) 1.0 eV(LDA), 0.7 eV(PBE)		
Context	B_g	$T_{i,As}$ (barrier?)	H	$T_{i,Al}$	$T_{i,As}$	H (barrier)	$T_{i,Al}$
LDA	0	+0.57	0.37	+0.10	+0.32	+1.01	0
PBE	0	+0.57	0.36	+0.15	+0.22	+0.72	0

2.4.3. Athermal and recombination enhanced diffusion: arsenic interstitial

The arsenic interstitial will likely diffuse athermally in *p*-type. One Bourgoin-Corbett migration path emerges from the search for ground state structures, diffusion driven by capture of carriers:



as the tetrahedral interstitial ground state captures an electron and collapses downhill, without a barrier, to the *H* site, which, in turn, re-emits the electron, and collapses downhill, without a barrier back into a *T* site. The complication is that B_g -site is the ground state for the (2+) charge state, and complicates this picture. There are further paths that capture yet more electrons and then insert into the lattice, and then re-emerge into different *T* site upon re-emitting their electrons. The relatively flat landscape and multiple bistabilities and changes in structure for the (1-), (0), and (1+) charge states further suggest that recombination enhanced diffusion is likely among these charge states of the arsenic interstitial.

This page intentionally left blank

3. CONCLUSIONS

The parameters needed to describe the defect properties of simple intrinsic defects in AIAs are summarized into Tables, tabulating the numerical results presented in PAS11.

4. REFERENCES

1. P.A. Schultz, MRS Symp. Proc. **1370**, mrss11-1370-yy03-04 doi:10.1557/opl.2011.765 (2011).
2. P.A. Schultz, Phys. Rev. Lett. **96**, 246401 (2006).
3. P.A. Schultz and O.A. von Lilienfeld, Modelling Simul. Mater. Sci. Eng. **17**, 084007 (2009).
4. SEQQUEST code, unpublished, <http://dft.sandia.gov/quest/>
5. J.P. Perdew and A. Zunger, Phys. Rev. **23**, 5048 (1981).
6. J.P. Perdew, K. Burke, and M. Ernzerhof, Phys. Rev. Lett. **77**, 3865 (1996).
7. A.E. Mattsson, P.A. Schultz, M.P. Desjarlais, T.R. Mattsson, and K. Leung, Modelling Simul. Mater. Sci. Eng. **13**, R1 (2005).
8. P.A. Schultz, Phys. Rev. B **60**, 1551 (1999).
9. O.A. von Lilienfeld and P.A. Schultz, Phys. Rev. B **77**, 115202 (2008).
10. A.E. Mattsson, R. Armiento, P.A. Schultz, and T.R. Mattsson, Phys. Rev. B **73**, 195123 (2006).
11. R.P. Leavitt and F.T. Towner, Phys. Rev. B **48**, 9154 (1993).
12. R.G. Green, H. Luo, T. Li, and A.L. Ruoff, Phys. Rev. Lett. **72**, 2045 (1994).
13. C.A. Mead and W.G. Spitzer, Phys. Rev. Lett. **11**, 358 (1963).
14. D.R. Lide (ed.), *Handbook of Chemistry and Physics*, 72nd Ed. (Boca Rotan: CRC Press, 1991).
15. W. Jost, J. Chem. Phys. **1**, 466 (1933).
16. R.E. Fern and A. Onton, J. Appl. Phys. **42**, 3499 (1971).
17. G.D. Watkins, in *Radiation Damage in Semiconductors*, ed. P. Baruch, p97 (Paris:Dunod, 1965).
18. J.C. Bourgoin and J.W. Corbett, Phys. Lett. A **38**, 135 (1972).

DISTRIBUTION

(to be distributed electronically)

1	MS0899	Technical Library	9536 (electronic copy)
1	MS1179	L. J. Lorence	1341 (ljloren@sandia.gov)
1	MS1056	W. R. Wampler	1111 (wrwampl@sandia.gov)
1	MS1323	E. R. Keiter	1445 (erkeite@sandia.gov)
1	MS1315	J. S. Nelson	1131 (jsnelso@sandia.gov)
1	MS1189	T. R. Mattsson	1641 (trmatts@sandia.gov)
1	MS0457	R. A. Paulsen	2211 (rapauls@sandia.gov)
1	MS1415	A. F. Wright	1131 (afwrigh@sandia.gov)

